Cr doping induced negative transverse magnetoresistance in Cd_3As_2 thin films

Yanwen Liu,[1,2] Rajarshi Tiwari,[3] Awadhesh Narayan,[3,4,5] Zhao Jin,[6] Xiang Yuan,[1,2] Cheng Zhang,[1,2] Feng Chen,[1,2] Liang Li,[6] Zhengcai Xia,[6] Stefano Sanvito,[3,*] Peng Zhou,[8,†] and Faxian Xiu[1,2,7,‡]

[1]*State Key Laboratory of Surface Physics and Department of Physics, Fudan University, Shanghai 200433, China*
[2]*Institute for Nanoelectronic Devices and Quantum Computing, Fudan University, Shanghai 200433, China*
[3]*School of Physics, AMBER and CRANN Institute, Trinity College, Dublin 2, Ireland*
[4]*Department of Physics, University of Illinois at Urbana-Champaign, Champaign, Illinois USA, 61801*
[5]*Materials Theory, ETH Zurich, Wolfgang-Pauli-Strasse 27, CH 8093, Zurich, Switzerland*
[6]*Wuhan National High Magnetic Field Center, Huazhong University of Science and Technology, Wuhan 430074, China*
[7]*Collaborative Innovation Center of Advanced Microstructures, Nanjing 210093, China*
[8]*State Key Laboratory of ASIC and System, Department of Microelectronics, Fudan University, Shanghai 200433, China*

(Received 17 August 2017; published 9 February 2018)

The magnetoresistance of a material conveys various dynamic information about charge and spin carriers, inspiring both fundamental studies in physics and practical applications such as magnetic sensors, data storage, and spintronic devices. Magnetic impurities play a crucial role in the magnetoresistance as they induce exotic states of matter such as the quantum anomalous Hall effect in topological insulators and tunable ferromagnetic phases in dilute magnetic semiconductors. However, magnetically doped topological Dirac semimetals are hitherto lacking. Here, we report a systematic study of Cr-doped Cd_3As_2 thin films grown by molecular-beam epitaxy. With the Cr doping, Cd_3As_2 thin films exhibit unexpected negative transverse magnetoresistance and strong quantum oscillations, bearing a trivial Berry's phase and an enhanced effective mass. More importantly, with ionic gating the magnetoresistance of Cr-doped Cd_3As_2 thin films can be drastically tuned from negative to positive, demonstrating the strong correlation between electrons and the localized spins of the Cr impurities, which we interpret through the formation of magnetic polarons. Such a negative magnetoresistance under perpendicular magnetic field and its gate tunability have not been observed previously in the Dirac semimetal Cd_3As_2. The Cr-induced topological phase transition and the formation of magnetic polarons in Cd_3As_2 provide insights into the magnetic interaction in Dirac semimetals as well as their potential applications in spintronics.

DOI: 10.1103/PhysRevB.97.085303

I. INTRODUCTION

It is well known that magnetic doping can effectively manipulate the magnetoresistance (MR) of a material and can possibly give rise to magnetism [1–4]. One notable example is that of dilute magnetic semiconductors, which combine in the same material the advantages of semiconductors and ferromagnets [1,3]. For instance, Mn substitution in GaAs provides a compound, (Ga,Mn)As, that exhibits negative MR and carrier-mediated ferromagnetism, and several other magnetically doped semiconductors and oxides have demonstrated novel spintronic functionalities [3,4]. Another important example is magnetically doped topological insulators (TIs). The topologically nontrivial ferromagnetic phase and the magnetic quantum-phase transition to a paramagnetic trivial state have been, respectively, demonstrated in different TI systems when increasing the magnetic doping [5]. The interplay between topological protection and the breaking of the time-reversal symmetry by the magnetic impurity results in intricate MR behavior in TI thin films, such as the competition between weak antilocalization (WAL) and weak localization (WL) [6,7]. More importantly, a quantum anomalous Hall effect has been achieved by means of magnetic doping and proper Fermi-level engineering [8–13].

At the same time, the great success of graphene and topological insulators [14–17] has generated a tremendous interest in topologically protected semimetals. Hereinto, the existence of Dirac semimetals, which host three-dimensional Dirac fermions in the bulk state, has been theoretically predicted and experimentally verified [18–22]. Among them, Cd_3As_2 was identified to be an ideal Dirac semimetal, showing good chemical stability [21], extremely high mobility [22–24], and chiral anomaly induced negative MR [25–28]. The robust topological protection in Cd_3As_2 has also been proved in different geometries like bulk [22–24], mircobelts [25,29], nanowires [26–28], and thin films [30], making this material conveniently exploited. When either the time-reversal symmetry or the inversion symmetry is broken, the degenerate Dirac nodes in a Dirac semimetal will separate into Weyl nodes, resulting in a Weyl semimetal phase. While inversion-symmetry-broken Weyl semimetals were realized in noncentrosymmetric monosphides from the TaAs family [31–33], stable time-reversal symmetry-broken Weyl semimetals without coupling to orbital motion and spin through Landau quantization and Zeeman splitting are still being sought. An external magnetic

*Sanvitos@tcd.ie
†pengzhou@fudan.edu.cn
‡Faxian@fudan.edu.cn

field or magnetic doping can implement the breaking of the time-reversal symmetry. A few theoretical studies have predicted a Ruderman-Kittel-Kasuya-Yosida interaction and a Kondo effect among the magnetic impurities in both Dirac and Weyl semimetals [34–37], although the experimental evidence remains lacking.

Here we report a systematic study of the magnetotransport properties of Cd_3As_2 thin films incorporating different concentrations of Cr doping. Our high-quality Cd_3As_2 thin films were grown by molecular-beam epitaxy (MBE), and a negative transverse MR is observed in all magnetically doped samples, suggesting that the doping induces spin-dependent scattering from magnetic polarons. The evolution of the Shubnikov–de Haas quantum oscillations indicates that the band structure and the topological properties experience a topological quantum-phase transition from a nontrivial to a trivial phase, a phase transition that is triggered by the Cr doping. Remarkably, the MR can be electrically manipulated via ionic gating and the resulting switching between positive and negative MR serves as a signature of magnetic polaron formation in Cr-doped Cd_3As_2. These findings are in a good agreement with density-functional theory and Monte Carlo calculations. Our results represent a step toward the manipulation of the topological Dirac semimetal phase via magnetic doping, and pave the way for potential spintronic applications of topological Dirac semimetals.

II. EXPERIMENTAL AND COMPUTATIONAL DETAILS

Cd_3As_2 thin films were grown in a CREATEC molecular beam epitaxy (MBE) system with base pressure less than 2×10^{-10} mbar. High-purity Cd (99.9999%), As (99.9999%), and Cr (99.9999%) were evaporated by dual-filament, valve-cracker, and single-filament effusion cells, respectively. Freshly cleaved mica substrates were annealed at 350 °C for 30 min to remove the molecule absorption. During the growth process, the substrate temperature was kept at 225 °C. The entire growth was *in situ* monitored by the reflection high-energy electron diffraction system. The crystal structure was determined by x-ray diffraction (Bruker D8 Discovery, Bruker Inc., Billerica, MA, USA).

The thin films were patterned into standard Hall bar geometry manually. The solid electrolyte was produced as follows: $LiClO_4$ (Sigma-Aldrich) and poly(ethylene oxide) ($M_w = 100\,000$, Sigma-Aldrich) powders were mixed with anhydrous methanol (Alfa Aesar). The solution was stirred overnight at 60 °C and served as the electrolyte. After the application of solid electrolyte, the device was kept at 350 K for 30 min in vacuum to remove the moisture before the transport measurements.

The magnetotransport measurements were performed in a Physical Property Measurement System by Quantum Design with a magnetic field up to 9 T. A home-made measurement system including lock-in amplifiers (Stanford Research 830) and Agilent 2912 source meters was used to acquire experimental data. Pulsed magnetic-field measurements up to 60 T were performed at Wuhan National High Magnetic Field Center.

Density-functional-theory calculations were carried out by employing the Perdew-Burke-Ernzerhof form of the exchange-correlation functional [38] as implemented in the QUANTUM ESPRESSO code [39]. The rotationally invariant form of the Hubbard U correction was used [40]. A plane-wave cutoff of 545 eV was employed and the Brillouin zone was sampled using an $8 \times 8 \times 4k$-point grid for the self-consistent calculations. The $I41/acd$ space group with an 80-atom unit cell for Cd_3As_2 was used [41].

III. RESULTS AND DISCUSSION

A. Growth and temperature-dependent resistance

Cd_3As_2 thin films were grown by MBE with different Cr doping concentrations. From our previous study we know that undoped Cd_3As_2 thin films thinner than 50 nm will experience a band-gap opening and become trivial insulators [30,42]. Therefore, we primarily focus on Cd_3As_2 thin films with a thickness of about 100 nm, which is thick enough to hold the Dirac feature. The Cr concentration can be fine-tuned by adjusting the Cr evaporation temperature during the growth (as discussed in the above experimental and computational details). The composition of as-grown thin films is determined by energy-dispersive x-ray spectroscopy (EDX). It is found that Cr replaces Cd and yields the compound $Cr_xCd_{3-x}As_2$ [43]. The single crystallinity with the growth face of (112) plane of the as-grown thin films is examined by x-ray diffraction (XRD) [Fig. 1(a)]. Standard Hall bar devices were built from the thin films. The temperature-dependent residual resistance $R(T)/R(300\,\mathrm{K})$ reveals the effect of the Cr doping. For undoped thin films, the resistance increases as the temperature decreases in the high-temperature regime and saturates at low temperatures. As the Cr concentration increases, however, the samples begin to exhibit a low-temperature metallic behavior, similar to what was reported for half metals [44].

B. MR behavior of the Cr-doped Cd_3As_2 thin films

To better understand the effect of the doping, we have performed temperature-dependent MR measurements of different Cr-doped Cd_3As_2 thin films. The most striking feature arising from the Cr substitution is the doping induced negative MR. In order to reveal the intrinsic effect of the magnetic doping, several representative samples are selected for the detailed study (Fig. 2). The undoped sample exhibits several prominent features of MR behavior [Fig. 2(a)], distinct from the extremely large MR ratio observed in the bulk counterpart [22,24]. Around zero field, there is a small dip in the MR, ascribed to WAL, which is also observed in Cd_3As_2 nanostructures [26–29]. Such MR behavior is reminiscent of the WAL in TIs and topological crystalline insulators [45,46]. According to the recent theoretical predictions [47], the WAL in Dirac or Weyl semimetals originates from quantum interference, giving a positive MR near zero field. Such a WAL phenomenon has been observed in TaAs [32,48] and regarded as a transport signature of Dirac and Weyl semimetals, apart from the chiral anomaly [26,28,32,47–49]. With increasing the magnetic field, the positive MR caused by the classical cyclotron motion prevails over the quantum interference effect and the quantum oscillations are clearly identified. This suggests a high mobility exceeding $2500\,\mathrm{cm^2V^{-1}s^{-1}}$, a value that is consistent with the measured Hall mobility of $2300\,\mathrm{cm^2V^{-1}s^{-1}}$ (Supplemental Material, Fig. 2 [50]).

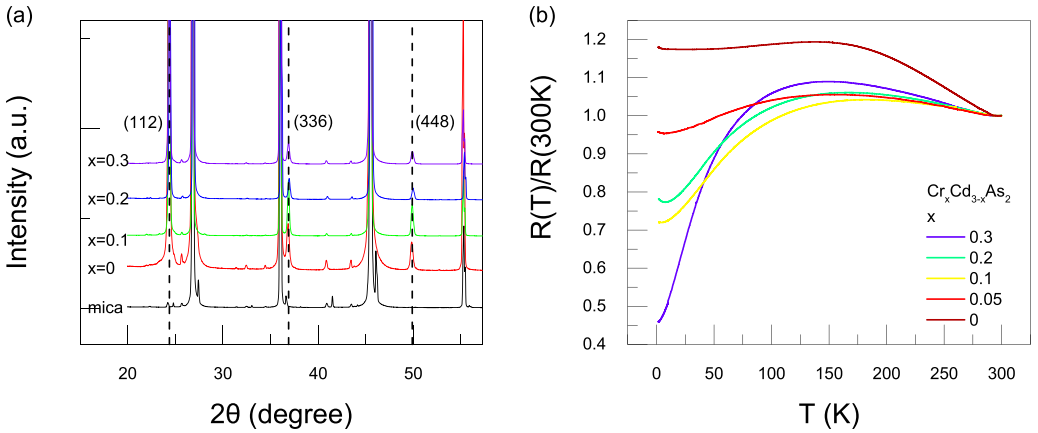

FIG. 1. The temperature-dependent resistance of different Cr-doped Cd_3As_2 thin films. (a) XRD spectra of as-grown thin films at different doping concentration. (b) The temperature-dependent residual resistance of different samples. The heavily doped samples show metallic behavior at low temperatures.

Just a tiny amount of Cr dopants ($x < 0.05$) suppresses dramatically the positive MR and provides a strong negative contribution [Fig. 2(b)]. The fact that the WAL feature is still preserved at zero field strongly suggests that there is only a negligible change in the topology of Cd_3As_2 at a light magnetic doping. However, the negative MR accompanied by the strong quantum oscillations persists up to 9 T, implying another hidden mechanism rather than WL, which usually contributes near zero field [47].

In order to verify the negative MR, a high magnetic pulsed field up to 55 T was applied to different magnetically doped samples [Fig. 2(c)]. The lightly doped sample ($x \leqslant 0.1$) shows a negative MR below 10 T and then a largely suppressed positive MR under higher magnetic field. The heavily doped case, however, boosts the effect of the magnetic doping further. The heavily doped one ($x \geqslant 0.2$) exhibits a negative MR up to ~30 T with strong quantum oscillations. For magnetic fields larger than 30 T, all the magnetically doped thin films display

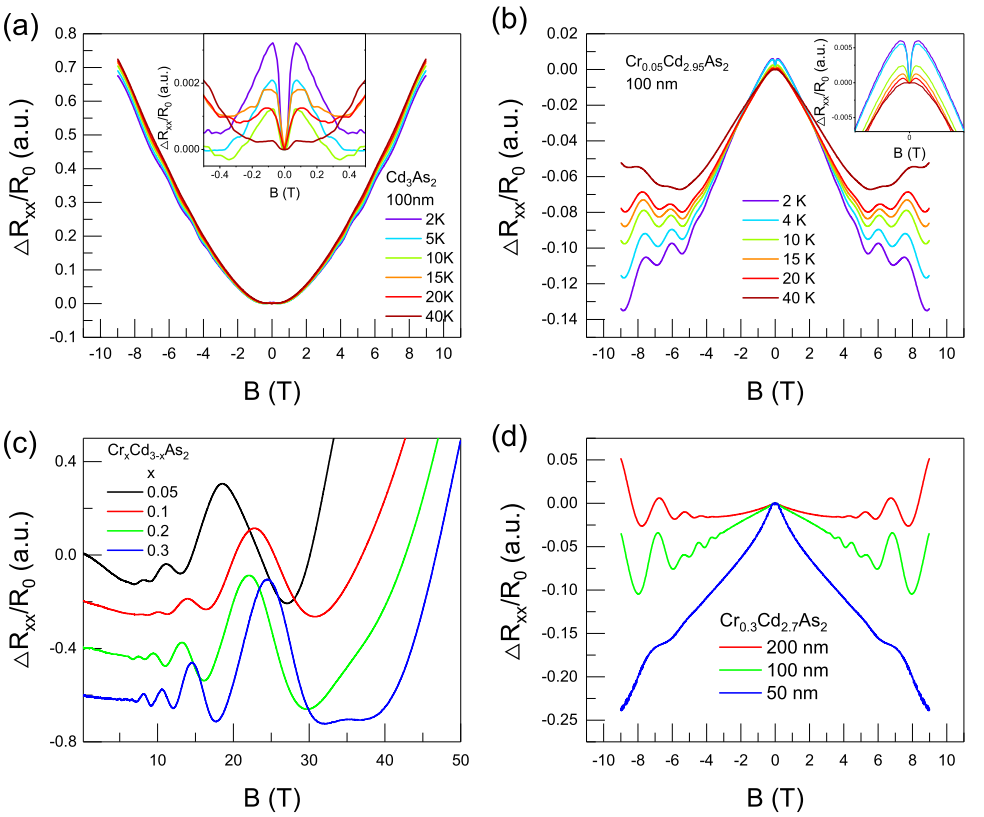

FIG. 2. MR behavior of different Cr-doped Cd_3As_2 thin films. (a), (b) The MR behavior at different temperatures for the undoped and lightly doped samples with the same thickness of 100 nm. (c) The MR behavior of different doping samples under ultrahigh magnetic pulsed field. (d) The thickness-dependent MR behavior for the heavily doped samples at 2 K.

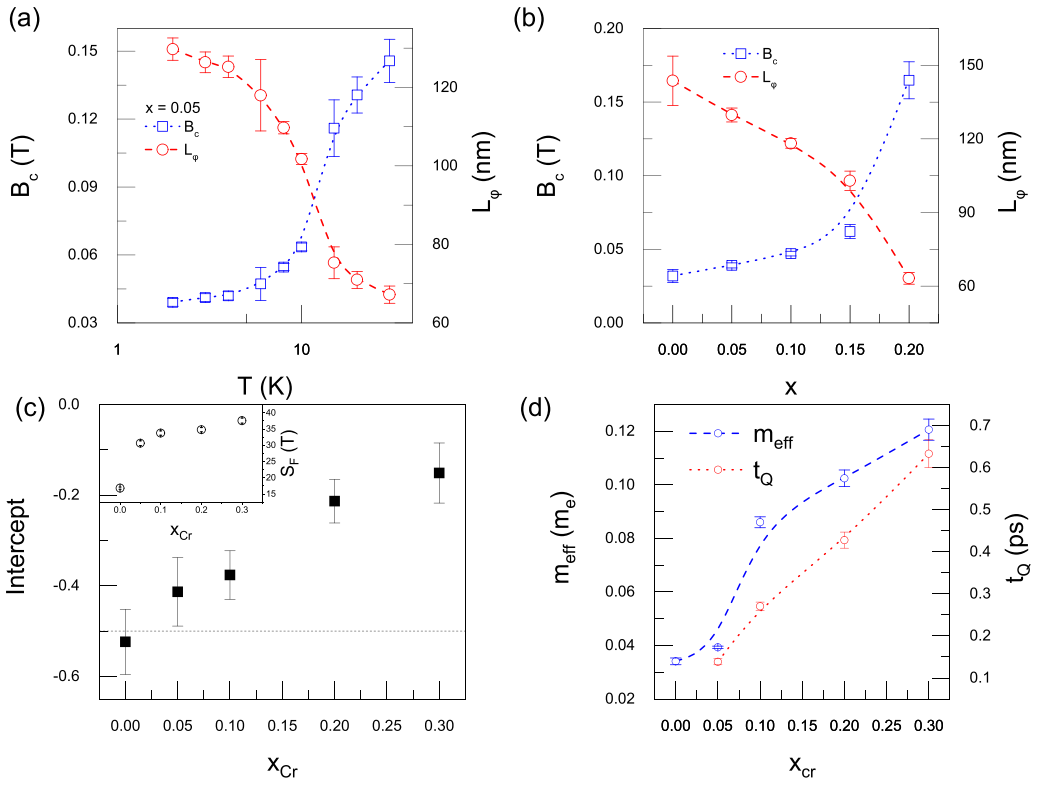

FIG. 3. Analysis of quantum oscillations. (a) The critical field and phase-coherence length of the lightly doped sample. (b) The critical field and phase-coherence length of the different Cr doping samples at 2 K. (c) The Berry phase of the different doping samples, indicating the quantum-phase transition from nontrivial to trivial state. The inset is doping-dependent oscillation frequencies. The error bars were generated from the linear fitting process in the Landau fan diagrams. (d) The effective mass of different samples, suggesting that the Cr doping enhances the effective mass. The quantum lifetime is extracted from the high-field quantum oscillations.

a rapidly growing positive MR, indicating that the system approaches the quantum limit as all the carriers are condensed into the lowest Landau level [51–53]. Such MR behavior in the quantum limit is confirmed by our following analysis of the quantum oscillations and is consistent with what was also reported in Cd_3As_2 nanowires with low carrier density [26,27].

The thickness-dependent MR of heavily doped samples shows that the dimensionality serves as an additional factor influencing the magnetotransport. The MR of the thin films with a thickness of 50, 100, and 200 nm was measured, as shown in Fig. 2(d). The negative MR ratio of the 50 nm sample at 9 T is about 25%, while for the thicker samples of 100 and 200 nm it is 10 and 2%, respectively. The thinner sample gives a larger negative MR, showing that with reducing the dimensionality the transport charges have much stronger interaction with the local magnetic moment [4].

C. Localization analysis

In order to gain a quantitative understanding of the competition between WAL and the negative MR induced by the Cr doping, we have extracted the phase-coherence length of different Cr-doped Cd_3As_2 thin films (Supplemental Material, Sec. 2 and Supplemental Material, Figs. 4 and 5), following the formula for 3D Dirac or Weyl semimetals [49]:

$$\Delta\sigma_{xx}^{qi} = C_1^{qi}\frac{B^2\sqrt{B}}{B_c^2+B^2} + C_2^{qi}\frac{B_c^2+B^2}{B_c^2+B^2}.$$

Here the parameters C_1^{qi} and C_2^{qi} are positive for WL and negative for WAL, and the critical field B_c is related to the phase-coherence length ℓ_ϕ according to $B_c \sim \hbar/e\ell_\phi^2$. The phase-coherence length ℓ_ϕ decreases from ~150 to ~60 nm with increasing Cr doping, directly suggesting the Cr-induced suppression of the WAL [Fig. 3(a)]. The temperature-dependent ℓ_ϕ of the lightly doped sample displays an abnormal evolution [Fig. 3(b)]. The ℓ_ϕ saturates at low temperature, similar to the case of dilute fluorinated graphene, having spin-flip states induced by the local magnetic moment [54].

D. Quantum oscillations analysis

Quantum oscillations provide a wealth of information about the band structure and the topological properties of materials. The oscillation frequency S_F is related to the area of the Fermi surface and the Berry's phase Φ_B is related to the topological property, which can be extracted from Landau fan diagrams according to the Lifshitz-Onsager quantization rule [55]: $\frac{S_F}{B} = N + \frac{1}{2} - \frac{\Phi_B}{2\pi} - \delta = N + \gamma$, where N is the Landau level index, S_F is obtained from the slope of the Landau fan diagram, and γ is the intercept. Conductivity σ_{xx} is converted from ρ_{xx} and ρ_{xy} using $\sigma_{xx} = \rho_{xx}/(\rho_{xx}^2 + \rho_{xy}^2)$. Here, the integer indices N denote the $\Delta\sigma_{xx}$ minima positions in $1/B$, while the half-integer indices represent the $\Delta\sigma_{xx}$ maxima positions. For Dirac fermions, the linear plot of $1/B$ vs N intercepts the N axis at 0.5, which implies a nontrivial π Berry's phase, whereas a value of around zero represents a

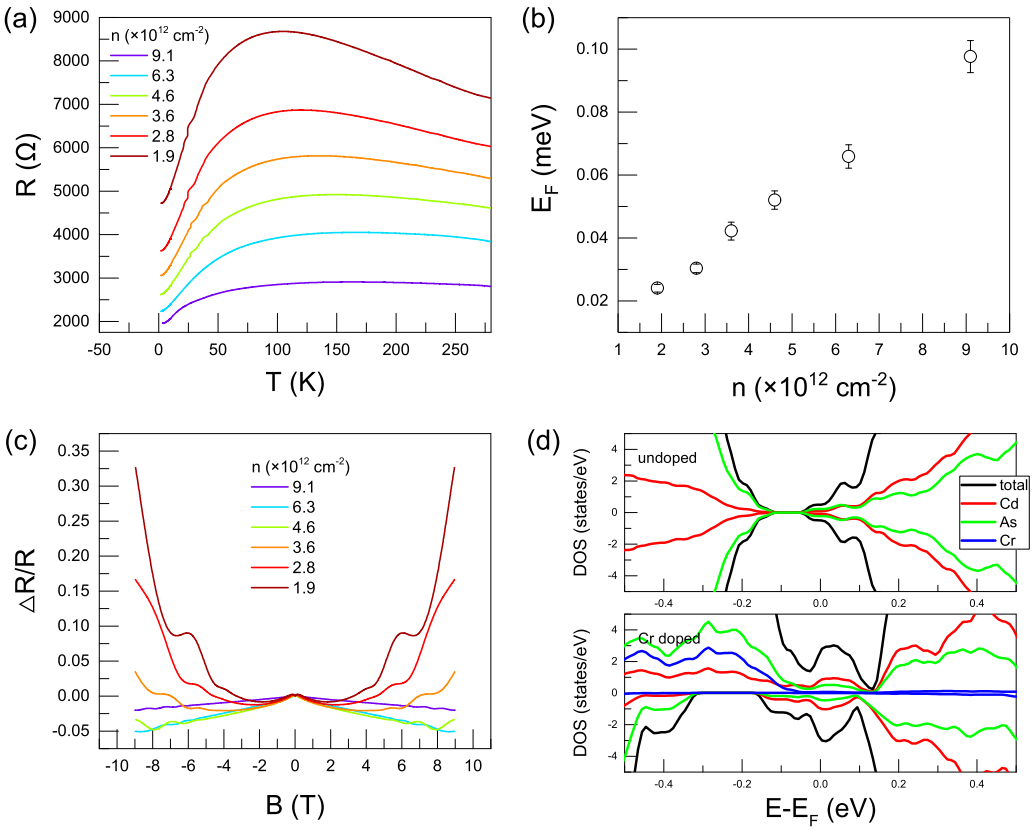

FIG. 4. Gate modulation of the magnetoresistance of the heavily doped sample. (a) The temperature-dependent resistance of different carrier density. (b) The Fermi energy as a function of carrier density. (c) The MR behavior with different carrier density. (d) Density of states of the undoped and Cr-doped samples (the Cr concentration is ∼4%).

trivial Berry's phase [23,56,57]. The measured S_F of different Cr-doped Cd_3As_2 thin films increases from ∼17 to ∼37 T, suggesting the doping induced larger Fermi surface [Fig. 3(c)]. The intercepts provide evidence for a Berry phase transition from nontrivial (the undoped sample) to trivial (the heavily doped sample), unambiguously showing the topological phase transition [Fig. 3(c)].

Such a quantum topological phase transition is also confirmed by the effective mass of charge carriers in the thin films. Following the Lifshitz-Kosevich formula [55,58,59], the oscillation component ΔR_{xx} could be described by

$$\Delta R_{xx} \propto R_T R_D \cos 2\pi \left(\frac{S_F}{B} + \gamma \right), \tag{1}$$

where R_T and R_D are the reduction factors accounting for the phase-smearing effects due to temperature and scattering, respectively. The effective mass m^* can be estimated from the temperature-dependent oscillation ΔR_{xx} according to the temperature-smearing factor $R_T \propto \frac{2\pi^2 k_B T m^*/\hbar eB}{\sinh(2\pi^2 k_B T m^*/\hbar eB)}$, where k_B is the Boltzmann's constant, $\hbar$ is the reduced Planck's constant (Supplemental Material, Fig. 6). The resulting effective mass of carriers in different Cr-doped Cd_3As_2 thin films can be extracted [Fig. 3(d)]. It is clear that the effective mass increases from $0.03\,m_e$ to $0.12\,m_e$ with high Cr concentration. Such a heavy effective mass in the heavily doped samples deviates from the usual small mass in Dirac systems, reconfirming the topological phase transition.

The carrier lifetime τ could be obtained from the Dingle factor $R_D \sim e^{-D}$, where $D = \frac{\pi m^*}{eB\tau}$. Because of the complicated MR background in small magnetic field, we have calculated the quantum lifetime from the high-field data of Fig. 2(f) for better accuracy (Supplemental Material, Fig. 7). Uncharacteristically, the quantum lifetime becomes longer as we increase the Cr concentration. The quantum lifetime indicates the small-angle scattering that dephases the momentum eigenstates of the carriers and is sensitive to all processes related to the Landau level broadening [22,23]. In fact, this could be directly witnessed from the much sharper quantum oscillations of the heavily doped samples than that of the undoped and lightly doped ones. Scattering from the Cr impurities in turn decreases the transport lifetime, which could be proved by the declining trend of the Hall mobility [Fig. 3(d)]. As Cr replaces the Cd ions, the spin-orbit interaction between Cd and As is significantly reduced, resulting in an increase of spin lifetime. Meanwhile, the local magnetic moment induced by the Cr impurities results in a series of well-resolved spin-polarized subbands under magnetic field [4], instead of the degenerated Landau levels as in the undoped sample. As a result, the scattering is reduced by the alignment of spins through the external magnetic field, giving rise to the enhanced quantum oscillations with relatively long quantum lifetime.

E. Gate-tunable MR behavior

In order to gain further insight into the mechanism leading to the negative MR by Cr doping, ionic gating has been applied to the heavily doped thin films. Previously, gate-tunable quantum oscillations and ambipolar effect have been demonstrated in undoped Cd_3As_2 thin films [42]. As the carrier density decreases, the resistance of the thin film increases, which is consistent with the electron-dominated transport [Fig. 4(a)]. The Fermi energy extracted from the quantum oscillations decreases from ∼100 to ∼20 meV, indicative of a good tunability of the heavily doped thin films. Moreover, as the Fermi level moves toward the bottom of the conduction band, the MR turns from entirely negative to positive [Fig. 4(c)], showing a similar behavior as that of the undoped sample [Fig. 2(a)]. Consequently, the effect of Cr doping is weakened gradually when the carrier density decreases, or when the Fermi level moves away from the conduction band. This indicates that the Cr doping generates an effective impurity band inside the conduction band. At low temperatures, the Fermi level lies inside this impurity band and the negative MR plays the dominant role. When the Fermi level is shifted away from the conduction band by the ionic gating, it leaves this impurity band, leading to the suppression of the negative MR (Supplemental Material, Fig. 10). This model is also supported by our density functional theory calculations as shown in Fig. 4(d). For undoped Cd_3As_2, the projected density of states (DOS) shows a band gap of about 0.1 eV, which is bridged by the Dirac cone (not displayed here) as observed in the band structure. In contrast, in the heavily doped samples [see lower panel of Fig. 4(d)], a band emerges in the DOS at the bottom of the conduction band, consistent with our experimental observations. Such a band originates from the *p-d* interaction between the Cr dopants and the valence band of the native Cd_3As_2 crystal, and there is a significant spin splitting of the bands. Such a mechanism is similar to other conventional diluted magnetic semiconductors, such as (Ga,Mn)As [4].

It is now fundamental to explore the mechanism behind the negative MR in our magnetically doped samples. From our experiments we find that the dopant concentration, the film thickness, and the carrier density can all affect the amplitude of the negative MR. In conventional ferromagnetic conductor, it is common to observe such negative MR due to the spin-dependent scattering [2]. However, in our samples, the ferromagnetism is not observed either in the transport or the magnetization measurements, and the same picture is confirmed by our Monte Carlo calculations (Supplemental Material, Figs. 4 and 9 and Supplemental Material, Sec. 3). According to the EDX analysis, the Cr impurities substitute for Cd in the Cd_3As_2. As a result, Cr impurities provide both local magnetic moments and hole doping. For the magnetism, the effective lattice is the Cd sublattice on which the localized spins of Cr lie. However, intrinsic defects in the thin films provide additional electron doping that compensates for the holes originating from Cr. Long-range magnetism can then be potentially activated by the *p-d* coupling, which is indeed strong as confirmed by our electronic structure analysis for Cr-doped crystals. However, the peculiar structure of the Cd_3As_2 lattice prevents the formation of a robust ferromagnetic ground state. The Cd sublattice presents little coordination (see detailed discussions in Supplemental Material, Sec. 4) so that the percolation threshold needed for long-range magnetism is reached only at a high Cr concentration [60]. We have estimated that such percolation threshold is approximately at 10% (10% of the Cd sites are substituted with Cr) for a fourth-nearest-neighbor Cr-Cr exchange interaction, a concentration far beyond what is present in our samples. Furthermore, even beyond the percolation threshold the critical temperature is driven by the long-distance exchange coupling, which we calculate to be small (see Supplemental Material, Table I). As such, even in the case percolation is reached through a spinodal arrangement of the Cr ions [61] the expected T_C remains low. In brief, our theoretical analysis returns Cr-doped Cd_3As_2 as a diluted paramagnet with a strong *p-d* coupling, namely it is similar to Mn-doped II-VI diluted semiconductors [62].

Monte Carlo simulations were applied to obtain the ferromagnetic transition temperature, T_C, over the entire range of Cr doping, where we use exchange parameters obtained from our first-principles calculations. For all the four cases from the first to the fourth neighbor, the long-range order is not generated until the Cr dopant reaches a percolation threshold at some critical concentrations of x_c. Here, x_c can reduce to 0.3 as one goes to a longer-range exchange including the fourth-neighbor exchange. As previously discussed, the introduction of Cr dopants suppresses the WAL behavior and generates a mechanism giving rise to the negative MR. The interplay between quantum localization and the magnetism is reminiscent of the magnetic polarons scenario in diluted semimetals and oxides [4,63,64]. Magnetic polarons are formed by the interaction between the carrier spins with the localized spins of the magnetic impurities [4]. Our electronic structure calculations showing a significant spin split of the valence band support the hypothesis of the magnetic polarons formation. Such polarons are likely to have a short polaron radius so that the percolation is not possible and no long-range ferromagnetic order is developed. Yet, the interaction between the transport electrons and the magnetic impurities remains strong and it can profoundly affect the transport properties. With the magnetic field, the spins between adjacent polarons are aligned well along the field direction. Also, the random spin of intermediate regions between magnetic polarons may be aligned with the increasing magnetic field. As a result, the spin-dependent scattering by the magnetic polarons is suppressed, leading to a negative contribution to the magnetoresistance.

Such a scenario can be also made plausible by several pieces of evidence from our transport data. It has been demonstrated that the magnetic polaron is favored by reducing the dimensionality of systems and by increasing the exchange constant and carrier effective mass [4]. In our experiments with the thinner samples the negative MR is more pronounced, whereas in the heavily doped 400-nm-thick sample, which is the 3D case, the negative MR is almost undetectable (Supplemental Material, Fig. 8 and Supplemental Material, Sec. 1). In thin films less than 100 nm thick, however, the negative MR dominates the transport, suggesting the formation of magnetic polarons in a quasi-2D case with the reducing thickness. All the heavily doped thin films have a large effective mass exceeding $0.1\,m_e$. This is a fingerprint of the formation of magnetic polarons. The second evidence is the carrier-density-dependent MR behavior in the heavily doped sample. By decreasing the carrier density through ionic gating, we observe the decrease of negative MR

and finally a revival of the positive MR with the carrier density of $\sim 2 \times 10^{12}\,\mathrm{cm}^{-2}$. With low carrier density, the strength of interaction between the carriers and magnetic impurities is greatly suppressed, suppressing the magnetic polarons, similar to the gate-tunable ferromagnetism in the MnGe quantum dots [65]. Consequently, quantum interference between electrons resumes the dominant role and the WAL emerges again.

IV. CONCLUSION

In conclusion, we have systemically studied the transport properties of Cr-doped Cd_3As_2 thin films. Magnetotransport measurements were performed for the films with different doping level, thickness, and carrier density. The magnetic doping induced metallic behavior and negative MR were observed at low temperatures. From the analysis of quantum oscillations, we have demonstrated the doping induced topological quantum-phase transition from nontrivial Dirac semimetal to trivial dilute magnetic semimetal as the Cr doping increases. For the lightly doped sample, the robust Dirac feature is preserved, demonstrating that Cd_3As_2 is a good platform to study the magnetic interaction of Dirac fermions in 3D. In contrast, for the heavily doped samples the formation of magnetic polarons is ascribed as the mechanism for the negative MR. Our results not only provide a direction on the research of Dirac semimetals, but also bring insights to the potential spintronic applications based on topological Dirac semimetals.

ACKNOWLEDGMENTS

This work was supported by the National Key Research and Development Program of China (Grant No. 2017YFA0303302) and National Natural Science Foundation of China (Grants No. 11474058 and No. 61674040). F.X. acknowledges the support from the open project of Wuhan National High Magnetic Field Center (Grant No. PHMFF2015003). A.N. acknowledges support from ETH Zurich. S.S. and R.T. acknowledge support from the European Research Council (QUEST project) and from Science Foundation Ireland (Grant No. 14/IA/2624). Part of the sample fabrication was performed at Fudan Nano-fabrication Laboratory. Computational resources were provided by the Trinity Centre for High Performance Computing (TCHPC).

[1] T. Dietl and H. Ohno, Rev. Mod. Phys. **86**, 187 (2014).
[2] T. Dietl, J. Phys. Soc. Jpn. **77**, 031005 (2008).
[3] T. Dietl, Nat. Mater. **9**, 965 (2010).
[4] *Introduction to the Physics of Diluted Magnetic Semiconductors*, edited by J. A. Gaj and J. Kossut (Springer, Berlin, 2010).
[5] J. Zhang, C.-Z. Chang, P. Tang, Z. Zhang, X. Feng, K. Li, L. Wang, X. Chen, C. Liu, W. Duan, K. He, Q.-K. Xue, X. Ma, and Y. Wang, Science **339**, 1582 (2013).
[6] M. Liu, J. Zhang, C.-Z. Chang, Z. Zhang, X. Feng, K. Li, K. He, L.-l. Wang, X. Chen, X. Dai, Z. Fang, Q.-K. Xue, X. Ma, and Y. Wang, Phys. Rev. Lett. **108**, 036805 (2012).
[7] Z. Zhang, X. Feng, M. Guo, K. Li, J. Zhang, Y. Ou, Y. Feng, L. Wang, X. Chen, K. He, X. Ma, Q. Xue, and Y. Wang, Nat. Commun. **5**, 4915 (2014).
[8] C.-Z. Chang, J. Zhang, X. Feng, J. Shen, Z. Zhang, M. Guo, K. Li, Y. Ou, P. Wei, L.-L. Wang, Z.-Q. Ji, Y. Feng, S. Ji, X. Chen, J. Jia, X. Dai, Z. Fang, S.-C. Zhang, K. He, Y. Wang, L. Lu, X.-C. Ma, and Q.-K. Xue, Science **340**, 167 (2013).
[9] K. He, Y. Wang, and Q.-K. Xue, Natl. Sci. Rev. **1**, 38 (2014).
[10] X. Kou, L. Pan, J. Wang, Y. Fan, E. S. Choi, W.-L. Lee, T. Nie, K. Murata, Q. Shao, S.-C. Zhang, and K. L. Wang, Nat. Commun. **6**, 8474 (2015).
[11] Y. Fan, P. Upadhyaya, X. Kou, M. Lang, S. Takei, Z. Wang, J. Tang, L. He, L.-T. Chang, M. Montazeri, G. Yu, W. Jiang, T. Nie, R. N. Schwartz, Y. Tserkovnyak, and K. L. Wang, Nat. Mater. **13**, 699 (2014).
[12] X. Kou, Y. Fan, M. Lang, P. Upadhyaya, and K. L. Wang, Solid State Commun. **215–216**, 34 (2015).
[13] Y. Fan, X. Kou, P. Upadhyaya, Q. Shao, L. Pan, M. Lang, X. Che, J. Tang, M. Montazeri, K. Murata, L.-T. Chang, M. Akyol, G. Yu, T. Nie, K. L. Wong, J. Liu, Y. Wang, Y. Tserkovnyak, and K. L. Wang, Nat. Nanotechnol. **11**, 352 (2016).
[14] A. H. Castro Neto, N. M. R. Peres, K. S. Novoselov, and A. K. Geim, Rev. Mod. Phys. **81**, 109 (2009).
[15] T. O. Wehling, A. M. Black-Schaffer, and A. V. Balatsky, Adv. Phys. **63**, 1 (2014).
[16] M. Z. Hasan and C. L. Kane, Rev. Mod. Phys. **82**, 3045 (2010).
[17] X.-L. Qi and S.-C. Zhang, Rev. Mod. Phys. **83**, 1057 (2011).
[18] Z. K. Liu, B. Zhou, Y. Zhang, Z. J. Wang, H. M. Weng, D. Prabhakaran, S. K. Mo, Z. X. Shen, Z. Fang, X. Dai, Z. Hussain, and Y. L. Chen, Science **343**, 864 (2014).
[19] Z. Wang, H. Weng, Q. Wu, X. Dai, and Z. Fang, Phys. Rev. B **88**, 125427 (2013).
[20] Z. Wang, Y. Sun, X.-Q. Chen, C. Franchini, G. Xu, H. Weng, X. Dai, and Z. Fang, Phys. Rev. B **85**, 195320 (2012).
[21] Z. K. Liu, J. Jiang, B. Zhou, Z. J. Wang, Y. Zhang, H. M. Weng, D. Prabhakaran, S. K. Mo, H. Peng, P. Dudin, T. Kim, M. Hoesch, Z. Fang, X. Dai, Z. X. Shen, D. L. Feng, Z. Hussain, and Y. L. Chen, Nat. Mater. **13**, 677 (2014).
[22] T. Liang, Q. Gibson, M. N. Ali, M. Liu, R. J. Cava, and N. P. Ong, Nat. Mater. **14**, 280 (2015).
[23] A. Narayanan, M. D. Watson, S. F. Blake, N. Bruyant, L. Drigo, Y. L. Chen, D. Prabhakaran, B. Yan, C. Felser, T. Kong, P. C. Canfield, and A. I. Coldea, Phys. Rev. Lett. **114**, 117201 (2015).
[24] J. Cao, S. Liang, C. Zhang, Y. Liu, J. Huang, Z. Jin, Z.-G. Chen, Z. Wang, Q. Wang, J. Zhao, S. Li, X. Dai, J. Zou, Z. Xia, L. Li, and F. Xiu, Nat. Commun. **6**, 7779 (2015).
[25] C. Zhang, E. Zhang, W. Wang, Y. Liu, Z.-G. Chen, S. Lu, S. Liang, J. Cao, X. Yuan, L. Tang, Q. Li, C. Zhou, T. Gu, Y. Wu, J. Zou, and F. Xiu, Nat. Commun. **8**, 13741 (2017).
[26] H. Li, H. He, H.-Z. Lu, H. Zhang, H. Liu, R. Ma, Z. Fan, S.-Q. Shen, and J. Wang, Nat. Commun. **7**, 10301 (2016).
[27] C.-Z. Li, L.-X. Wang, H. Liu, J. Wang, Z.-M. Liao, and D.-P. Yu, Nat. Commun. **6**, 10137 (2015).
[28] L.-X. Wang, C.-Z. Li, D.-P. Yu, and Z.-M. Liao, Nat. Commun. **7**, 10769 (2016).
[29] Z.-G. Chen, C. Zhang, Y. Zou, E. Zhang, L. Yang, M. Hong, F. Xiu, and J. Zou, Nano Lett. **15**, 5830 (2015).

[30] P. Cheng, C. Zhang, Y. Liu, X. Yuan, F. Song, Q. Sun, P. Zhou, D. W. Zhang, and F. Xiu, New J. Phys. **18**, 083003 (2016).
[31] C.-L. Zhang, B. Tong, Z. Yuan, Z. Lin, J. Wang, J. Zhang, C.-Y. Xi, Z. Wang, S. Jia, and C. Zhang, Phys. Rev. B **94**, 205120 (2016).
[32] C.-L. Zhang, S.-Y. Xu, I. Belopolski, Z. Yuan, Z. Lin, B. Tong, G. Bian, N. Alidoust, C.-C. Lee, S.-M. Huang, T.-R. Chang, G. Chang, C.-H. Hsu, H.-T. Jeng, M. Neupane, D. S. Sanchez, H. Zheng, J. Wang, H. Lin, C. Zhang, H.-Z. Lu, S.-Q. Shen, T. Neupert, M. Zahid Hasan, and S. Jia, Nat. Commun. **7**, 10735 (2016).
[33] C.-L. Zhang, S.-Y. Xu, C. M. Wang, Z. Lin, Z. Z. Du, C. Guo, C.-C. Lee, H. Lu, Y. Feng, S.-M. Huang, G. Chang, C.-H. Hsu, H. Liu, H. Lin, L. Li, C. Zhang, J. Zhang, X.-C. Xie, T. Neupert, M. Z. Hasan, H.-Z. Lu, J. Wang, and S. Jia, Nat. Phys. **13**, 979 (2017).
[34] H.-R. Chang, J. Zhou, S.-X. Wang, W.-Y. Shan, and D. Xiao, Phys. Rev. B **92**, 241103 (2015).
[35] J.-H. Sun, D.-H. Xu, F.-C. Zhang, and Y. Zhou, Phys. Rev. B **92**, 195124 (2015).
[36] A. K. Mitchell and L. Fritz, Phys. Rev. B **92**, 121109 (2015).
[37] M. V. Hosseini and M. Askari, Phys. Rev. B **92**, 224435 (2015).
[38] J. P. Perdew, K. Burke, and M. Ernzerhof, Phys. Rev. Lett. **77**, 3865 (1996).
[39] P. Giannozzi, S. Baroni, N. Bonini, M. Calandra, R. Car, C. Cavazzoni, D. Ceresoli, G. L. Chiarotti, M. Cococcioni, I. Dabo, A. D. Corso, S. de Gironcoli, S. Fabris, G. Fratesi, R. Gebauer, U. Gerstmann, C. Gougoussis, A. Kokalj, M. Lazzeri, L. Martin-Samos, N. Marzari, F. Mauri, R. Mazzarello, S. Paolini, A. Pasquarello, L. Paulatto, C. Sbraccia, S. Scandolo, G. Sclauzero, A. P. Seitsonen, A. Smogunov, P. Umari, and R. M. Wentzcovitch, J. Phys.: Condens. Matter **21**, 395502 (2009).
[40] S. L. Dudarev, G. A. Botton, S. Y. Savrasov, C. J. Humphreys, and A. P. Sutton, Phys. Rev. B **57**, 1505 (1998).
[41] M. N. Ali, Q. Gibson, S. Jeon, B. B. Zhou, A. Yazdani, and R. J. Cava, Inorg. Chem. **53**, 4062 (2014).
[42] Y. Liu, C. Zhang, X. Yuan, T. Lei, C. Wang, D. Di Sante, A. Narayan, L. He, S. Picozzi, S. Sanvito, R. Che, and F. Xiu, NPG Asia Mater. **7**, e221 (2015).
[43] X. Yuan, P. Cheng, L. Zhang, C. Zhang, J. Wang, Y. Liu, Q. Sun, P. Zhou, D. W. Zhang, Z. Hu, X. Wan, H. Yan, Z. Li, and F. Xiu, Nano Lett. **17**, 2211 (2017).
[44] T. Guan, C. Lin, C. Yang, Y. Shi, C. Ren, Y. Li, H. Weng, X. Dai, Z. Fang, S. Yan, and P. Xiong, Phys. Rev. Lett. **115**, 087002 (2015).
[45] M. Lang, L. He, X. Kou, P. Upadhyaya, Y. Fan, H. Chu, Y. Jiang, J. H. Bardarson, W. Jiang, E. S. Choi, Y. Wang, N.-C. Yeh, J. Moore, and K. L. Wang, Nano Lett. **13**, 48 (2013).
[46] C. Zhang, Y. Liu, X. Yuan, W. Wang, S. Liang, and F. Xiu, Nano Lett. **15**, 2161 (2015).
[47] H.-Z. Lu and S.-Q. Shen, Phys. Rev. B **92**, 035203 (2015).
[48] X. Huang, L. Zhao, Y. Long, P. Wang, D. Chen, Z. Yang, H. Liang, M. Xue, H. Weng, Z. Fang, X. Dai, and G. Chen, Phys. Rev. X **5**, 031023 (2015).
[49] H.-Z. Lu and S.-Q. Shen, Front. Phys. **12**, 127201 (2017).
[50] See Supplemental Material at http://link.aps.org/supplemental/10.1103/PhysRevB.97.085303 for detailed analysis of quantum oscillations and theoretical calculations.
[51] A. A. Abrikosov, Phys. Rev. B **58**, 2788 (1998).
[52] A. A. Abrikosov, Europhys. Lett. **49**, 789 (2000).
[53] J. Hu and T. F. Rosenbaum, Nat. Mater. **7**, 697 (2008).
[54] X. Hong, K. Zou, B. Wang, S.-H. Cheng, and J. Zhu, Phys. Rev. Lett. **108**, 226602 (2012).
[55] H. Murakawa, M. S. Bahramy, M. Tokunaga, Y. Kohama, C. Bell, Y. Kaneko, N. Nagaosa, H. Y. Hwang, and Y. Tokura, Science **342**, 1490 (2013).
[56] J. Xiong, Y. Luo, Y. Khoo, S. Jia, R. J. Cava, and N. P. Ong, Phys. Rev. B **86**, 045314 (2012).
[57] Z. J. Xiang, D. Zhao, Z. Jin, C. Shang, L. K. Ma, G. J. Ye, B. Lei, T. Wu, Z. C. Xia, and X. H. Chen, Phys. Rev. Lett. **115**, 226401 (2015).
[58] D. Shoenberg, *Magnetic Oscillations in Metals* (Cambridge University Press, Cambridge, England, 1984).
[59] L. Li, G. J. Ye, V. Tran, R. Fei, G. Chen, H. Wang, J. Wang, K. Watanabe, T. Taniguchi, L. Yang, X. H. Chen, and Y. Zhang, Nat. Nanotechnol. **10**, 608 (2015).
[60] J. Osorio-Guillén, S. Lany, S. V. Barabash, and A. Zunger, Phys. Rev. B **75**, 184421 (2007).
[61] K. Sato, H. Katayama-Yoshida, and P. H. Dederichs, Jpn. J. Appl. Phys. **44**, L948 (2005).
[62] H. Saito, W. Zaets, S. Yamagata, Y. Suzuki, and K. Ando, J. Appl. Phys. **91**, 8085 (2002).
[63] J. M. D. Coey, M. Venkatesan, and C. B. Fitzgerald, Nat. Mater. **4**, 173 (2005).
[64] A. H. MacDonald, P. Schiffer, and N. Samarth, Nat. Mater. **4**, 195 (2005).
[65] F. Xiu, Y. Wang, J. Kim, P. Upadhyaya, Y. Zhou, X. Kou, W. Han, R. K. Kawakami, J. Zou, and K. L. Wang, ACS Nano **4**, 4948 (2010).